Constraints on the composition and temperature of LLSVPs from seismic properties of lower mantle minerals

Kenny Vilella[a,b,*], Thomas Bodin[c], Charles-Edouard Boukaré[d], Frédéric Deschamps[b], James Badro[e], Maxim Ballmer[f], Yang Li[g]

[a] *JSPS International Research Fellow, Hokkaido University, Japan*
[b] *Institute of Earth Sciences, Academia Sinica, Taipei, Taiwan*
[c] *Laboratoire de Géologie de Lyon, UMR 5276, Université de Lyon, Villeurbanne, France*
[d] *Earth and Planetary Science Laboratory, École Polytechnique Fédérale de Lausanne, Lausanne, Switzerland*
[e] *Institut de Physique du Globe, Univ. Paris Diderot, Sorbonne Paris Cité, CNRS, Paris, France*
[f] *Institute of Geophysics, Department of Earth Sciences, ETH Zurich, Zurich, Switzerland*
[g] *Key Laboratory of Earth and Planetary Physics, Institute of Geology and Geophysics, Chinese Academy of Science, Beijing, China*

Determination of the iron concentration

The definition of the Fe-Mg exchange coefficient between bridgmanite (Bm) and ferropericlase (Fp) gives that

$$K^{\mathrm{Bm-Fp}} = \frac{\left(\frac{\mathrm{Fe}}{\mathrm{Mg}}\right)_{\mathrm{Bm}}}{\left(\frac{\mathrm{Fe}}{\mathrm{Mg}}\right)_{\mathrm{Fp}}} = \frac{\frac{x_{\mathrm{Fe,Bm}}}{x_{\mathrm{Mg,Bm}}}}{\frac{x_{\mathrm{Fe,Fp}}}{x_{\mathrm{Mg,Fp}}}}, \tag{1}$$

where $x_{\mathrm{Fe,Bm}}$, $x_{\mathrm{Mg,Bm}}$, $x_{\mathrm{Fe,Fp}}$, $x_{\mathrm{Mg,Fp}}$ are the molar concentrations of MgO or FeO in Fp or Bm. Note that $x_{\mathrm{Mg,Fp}} = 1 - x_{\mathrm{Fe,Fp}}$ and that for the sake of simplicity we will write simply x_{Fp} and x_{Bm} instead of $x_{\mathrm{Fe,Fp}}$ and $x_{\mathrm{Fe,Bm}}$, respectively. Moreover,

$$x_{\mathrm{Mg,Bm}} = 0.5 x_{\mathrm{MgSiO_3}}, \tag{2}$$

*Corresponding author
Email address: kennyvilella@gmail.com (Kenny Vilella)

where the factor 0.5 indicates that $x_{\mathrm{MgSiO_3}}$ (the molar concentration of $MgSiO_3$ in Bm) is composed of both MgO and SiO_2. Considering the components in Bm, we can write that

$$\begin{aligned} x_{\mathrm{MgSiO_3}} &= 1 - x_{\mathrm{FeSiO_3}} - x_{\mathrm{FeAlO_3}} - x_{\mathrm{Al_2O_3}} - x_{\mathrm{Fe_2O_3}} && (3)\\ &= 1 - (2 - R_{\mathrm{Fe}})x_{\mathrm{Bm}} - x_{\mathrm{Al}}, && (4) \end{aligned}$$

with x_{Al} the molar concentration of AlO_2 in Bm, R_{Fe} =$\mathrm{Fe^{3+}}/\sum \mathrm{Fe}$, and $x_{\mathrm{FeSiO_3}}$, $x_{\mathrm{FeAlO_3}}$, $x_{\mathrm{Al_2O_3}}$, $x_{\mathrm{Fe_2O_3}}$, the molar concentration in Bm of $FeSiO_3$, $FeAlO_3$, Al_2O_3 and Fe_2O_3, respectively. Note that in case of alumina excess,

$$\begin{aligned} x_{\mathrm{FeSiO_3}} &= 2(1 - R_{\mathrm{Fe}})x_{\mathrm{Bm}} && (5)\\ x_{\mathrm{FeAlO_3}} &= 2\,R_{\mathrm{Fe}}\,x_{\mathrm{Bm}} && (6)\\ x_{\mathrm{Al_2O_3}} &= x_{\mathrm{Al}} - R_{\mathrm{Fe}}\,x_{\mathrm{Bm}} && (7)\\ x_{\mathrm{Fe_2O_3}} &= 0 && (8) \end{aligned}$$

while in case of iron excess,

$$\begin{aligned} x_{\mathrm{FeSiO_3}} &= 2(1 - R_{\mathrm{Fe}})x_{\mathrm{Bm}} && (9)\\ x_{\mathrm{FeAlO_3}} &= 2\,x_{\mathrm{Al}} && (10)\\ x_{\mathrm{Al_2O_3}} &= 0 && (11)\\ x_{\mathrm{Fe_2O_3}} &= R_{\mathrm{Fe}}\,x_{\mathrm{Bm}} - x_{\mathrm{Al}}. && (12) \end{aligned}$$

Eq. 1 gives therefore a relationship between x_{Bm}, x_{Fp} and x_{Al}, since R_{Fe} and $K^{\mathrm{Bm-Fp}}$ are input parameters. A second relationship is obtained considering another input parameter, $P_{\mathrm{Al_2O_3}}$, the amount of Al_2O_3 in the composition (wt%). Indeed,

$$P_{\mathrm{Al_2O_3}} = \frac{M_{\mathrm{Al_2O_3}}}{M_{\mathrm{Bm}}} X_{\mathrm{m,Bm}}\, x_{\mathrm{Al}}, \qquad (13)$$

with $M_{\mathrm{Al_2O_3}}$ the molar mass of Al_2O_3, which can be easily calculated, M_{Bm} the molar mass of Bm, $X_{\mathrm{m,Bm}}$ the mass fraction of Bm. The molar mass of Bm is

a function of x_{Al} and x_{Bm},

$$M_{\mathrm{Bm}} = x_{\mathrm{MgSiO_3}} M_{\mathrm{MgSiO_3}} + x_{\mathrm{FeSiO_3}} M_{\mathrm{FeSiO_3}} + x_{\mathrm{FeAlO_3}} M_{\mathrm{FeAlO_3}} + x_{\mathrm{Al_2O_3}} M_{\mathrm{Al_2O_3}} + x_{\mathrm{Fe_2O_3}} M_{\mathrm{Fe_2O_3}}, \tag{14}$$

where $M_{\mathrm{MgSiO_3}}$, $M_{\mathrm{FeSiO_3}}$, $M_{\mathrm{FeAlO_3}}$, and $M_{\mathrm{Fe_2O_3}}$ are the molar mass of $MgSiO_3$, $FeSiO_3$, $FeAlO_3$, and Fe_2O_3, respectively. In our approach, we assume that the volume proportion of minerals is constant with depth, to obtain the mass proportion $X_{\mathrm{m,Bm}}$ we can thus use,

$$X_{\mathrm{m,Bm}} = \frac{1}{1 + \frac{X_{\mathrm{vol,CaPv}}}{X_{\mathrm{vol,Bm}}} \frac{\rho_{\mathrm{CaPv}}}{\rho_{\mathrm{Bm}}} + \frac{X_{\mathrm{vol,Fp}}}{X_{\mathrm{vol,Bm}}} \frac{\rho_{\mathrm{Fp}}}{\rho_{\mathrm{Bm}}}}, \tag{15}$$

with $X_{\mathrm{vol,CaPv}}$, $X_{\mathrm{vol,Bm}}$ and $X_{\mathrm{vol,Fp}}$ the volume proportion of Ca-silicate perovskite (CaPv), Bm, and Fp, respectively, which are input parameters of our model, and ρ_{CaPv}, ρ_{Bm}, and ρ_{Fp} the density of CaPv, Bm, and Fp, respectively. These densities are additional unknowns that can be calculated using the Mie-Grüneisen-Debye equation of state. Inserting eqs 14 and 15 in eq 13, we obtain another relationship between x_{Bm}, x_{Fp} and x_{Al}. The last relationship is obtained considering P_{FeO}, the amount of FeO in the composition (wt%). More specifically, we use the fact that

$$\frac{P_{\mathrm{FeO}}}{P_{\mathrm{Al_2O_3}}} = \frac{M_{\mathrm{FeO}}}{M_{\mathrm{Al_2O_3}}} \frac{2\, X_{\mathrm{m,Bm}}\, M_{\mathrm{Fp}}\, x_{\mathrm{Bm}} + X_{\mathrm{m,Fp}}\, M_{\mathrm{Bm}}\, x_{\mathrm{Fp}}}{X_{\mathrm{m,Bm}}\, M_{\mathrm{Fp}}\, x_{\mathrm{Al}}}, \tag{16}$$

with $X_{\mathrm{m,Fp}}$ the mass proportion of Fp, M_{FeO} and M_{Fp} the molar mass of FeO and Fp, respectively. We finally obtain a system of six equations (eqs. 1, 13, 16 and the Mie-Grüneisen-Debye equation of state applied to each of the three minerals considered) and 6 unknowns (x_{Bm}, x_{Fp}, x_{Al}, ρ_{CaPv}, ρ_{Bm}, and ρ_{Fp}) that can be solved numerically. Note that these equations can be rearranged to obtain a system of three equations and three unknowns, making the calculation faster and more accurate.

Determination of the isentropic bulk modulus K_s

The isentropic bulk modulus K_s can be calculated using

$$K_s = K_T(1 + \alpha\gamma T), \tag{17}$$

where K_T is the isothermal bulk modulus, α the thermal expansion coefficient and,

$$\gamma = \gamma_0 \left(\frac{V}{V_0} \right)^q \tag{18}$$

the Grüneisen parameter, with V the volume and q a constant parameter. Note that the subscript 0 indicates that the property is taken at ambient conditions. The temperature derivative of the Mie-Grüneisen-Debye equation of state (Jackson and Rigden, 1996) implies that

$$\alpha = \frac{\gamma}{V\, K_T} \left(\frac{\partial \Delta E_{th}}{\partial T} \right)_V, \tag{19}$$

where

$$\Delta E_{th} = E_{th}(T) - E_{th}(T_0), \tag{20}$$

and

$$E_{th} = \frac{9nRT^4}{\theta^3} \int_0^{\theta/T} \frac{x^3}{\mathrm{e}^x - 1} \mathrm{d}x, \tag{21}$$

is the vibrational energy (calculated from the Debye model), with T the temperature, R the gas constant, n the number of atoms per formula unit, and

$$\theta = \theta_0\, \mathrm{e}^{\frac{\gamma_0 - \gamma}{q}}, \tag{22}$$

the Debye temperature. Finally, the temperature derivative of eq 20 gives

$$\left(\frac{\partial \Delta E_{th}}{\partial T} \right)_V = \frac{4E_{th}}{T} - \frac{9nR\theta}{T(\mathrm{e}^{\theta/T} - 1)}. \tag{23}$$

Furthermore, the volume derivative of the Mie-Grüneisen-Debye equation of state gives

$$K_T(V,T) = K_T(V,T_0) - (q-1)\frac{\gamma \Delta E_{th}}{V} - \gamma\left(\frac{\partial \Delta E_{th}}{\partial V}\right)_T, \tag{24}$$

where $K_T(V,T_0)$ is calculated with the volume derivative of the third order Birch-Murnaghan equation of state,

$$\begin{aligned} K_T(V,T_0) = \frac{3K_{T0}}{4}(K'_{T0}-4)\left(\frac{V_0}{V}\right)^{2/3}\left[\left(\frac{V_0}{V}\right)^{7/3} - \left(\frac{V_0}{V}\right)^{5/3}\right] + \\ \frac{K_{T0}}{2}\left\{1 + \frac{3}{4}(K'_{T0}-4)\left[\left(\frac{V_0}{V}\right)^{2/3} - 1\right]\right\}\left[7\left(\frac{V_0}{V}\right)^{7/3} - 5\left(\frac{V_0}{V}\right)^{5/3}\right], \end{aligned} \tag{25}$$

and the volume derivative of eq 20 writes

$$\left(\frac{\partial \Delta E_{th}}{\partial V}\right)_T = \frac{\gamma\theta}{V}\left(\frac{3\Delta E_{th}}{\theta} - 9nR\left[\frac{1}{e^{\theta/T}-1} - \frac{1}{e^{\theta/T_0}-1}\right]\right). \tag{26}$$

This set of relationships allows to calculate K_s at any (P,T) conditions as a function of V and mineral properties at ambient conditions. While the mineral properties at ambient conditions are reported in Tables 1 and 2, the volume V is obtained by solving the Mie-Grüneisen-Debye equation of state.

Spin state transition

The effect of the Fe^{2+} spin state transition in ferropericlase is calculated following Vilella et al. (2015), which is itself based on the theoretical work of Sturhahn et al. (2005). In this approach, we calculate the average Fe^{2+} spin configuration in Fp by minimizing the Helmholtz free energy: $F = U - TS$. Although it may be more realistic to minimize the Gibbs free energy, minimizing the Gibbs or Helmholtz free energy actually gives equivalent results, while considering the Gibbs free energy increases importantly the computational time. The internal energy is given by

$$U = -NJ_{\mathrm{LS}}\eta_{\mathrm{LS}}^2 + N(\eta_{\mathrm{LS}}E_{\mathrm{LS}} + \eta_{\mathrm{HS}}E_{\mathrm{HS}}), \tag{27}$$

where N is the number of Fe^{2+} in Fp, $E_{\rm LS}$ and $E_{\rm HS}$ are the energy levels of LS state and HS state, respectively, $J_{\rm LS}$ is the coupling LS state-LS state, $\eta_{\rm LS}$ and $\eta_{\rm HS}$ the fractions of Fe^{2+} in LS state and HS state, respectively, with $\eta_{\rm LS} + \eta_{\rm HS} = 1$. The entropy of the crystal can be written as

$$S = -k_B N \left[\eta_{\rm LS} \ln\left(\frac{\eta_{\rm LS}}{g_{\rm LS}}\right) + \eta_{\rm HS} \ln\left(\frac{\eta_{\rm HS}}{g_{HS}}\right) \right], \tag{28}$$

where k_B is the Boltzmann constant, $g_{\rm LS}$ and $g_{\rm HS}$ are the energy degeneracies of the electronic configuration. These expressions allows to obtain the fraction of iron in the LS state as a function of iron content, volume, and temperature.

Additional information on the reference composition

Following the nature of the available observations, constraints on LLSVPs can only be obtained relatively to the far-field mantle. As such, our choice for the reference composition has a critical importance. Here, we follow the traditional assumption of a pyrolitic mantle (McDonough and Sun, 1995). More specifically, we choose to consider the pyrolitic composition investigated by Irifune et al. (2010) and described in Tables 3 and 4. It is however important to note that different pyrolitic models have been suggested exhibiting slight compositional variations (e.g., see Table 3). In order to confirm the relevance of our reference composition, we report in Figure 6 the predicted density and seismic wave speed profiles compared to PREM. Note that we have accounted for the uncertainties on mantle temperatures (e.g., Deschamps and Trampert, 2004) by considering the geotherm of Brown and Shankland (1981) as a lower bound, and the geotherm from 3D numerical simulations (Vilella et al., 2015) as an upper bound. As shown in Figure 6, the calculated profiles for V_S and, to a lesser extent, V_P are underestimated by our model. The disagreement is higher at lower pressures, up to $\sim$6% and $\sim$2.5%, respectively, and vanishes at lowermost mantle condition. This disagreement is probably due to the uncertainties on the determination of the shear modulus. However, a key result of our work is that the constraints on the V_S and V_P anomalies of LLSVPs are much less efficient

than the ones on the density and V_ϕ to constrain the potential composition of LLSVPs. As a result, the crucial requirement for our reference composition is to predict reasonably well the density and bulk sound velocity of the lowermost mantle. While PREM density is perfectly reproduced by our reference composition (Figure 6c), the bulk sound velocity predicted is slightly lower than PREM (up to $\sim$1.5%). This may be due to the presence of MORB material in the lowermost mantle. Indeed MORBs are characterized by a higher bulk sound velocity than PREM (Wu et al., 2017), so that the presence of a MORB component may explain the difference between our calculated V_ϕ and the one estimated by PREM. We therefore conclude that our reference composition is compatible with available constraints.

Reference

Brown, J.M., Shankland, T.J., 1981. Thermodynamic parameters in the Earth as determined from seismic profiles. Geophysical Journal of the Royal Astronomical Society 66, 579–596. doi:10.1111/j.1365-246X.1981.tb04891.x.

Catalli, K., Shim, S.H., Dera, P., Prakapenka, V.B., Zhao, J., Sturhahn, W., Chow, P., Xiao, Y., Cynn, H., Evans, W.J., 2011. Effects of the Fe^{3+} spin transition on the properties of aluminous perovskite — new insights for lower-mantle seismic heterogeneities. Earth and Planetary Science Letters 310, 293–302. doi:10.1016/j.epsl.2011.08.018.

Catalli, K., Shim, S.H., Prakapenka, V.B., Zhao, J., Sturhahn, W., Chow, P., Xiao, Y., Liu, H., Cynn, H., Evans, W.J., 2010. Spin state of ferric iron in $MgSiO_3$ perovskite and its effect on elastic properties. Earth and Planetary Science Letters 289, 68–75. doi:10.1016/j.epsl.2009.10.029.

Deschamps, F., Trampert, J., 2004. Towards a lower mantle reference temperature and composition. Earth and Planetary Science Letters 222, 161–175. doi:10.1016/j.epsl.2004.02.024.

Fei, Y.W., Zhang, L., Corgne, A., Watson, H.C., Ricolleau, A., Meng, Y., Prakapenka, V.B., 2007. Spin transition and equations of state of (Mg, Fe)O solid solutions. Geophysical Research Letters 34, L17307. doi:10.1029/2007GL030712.

Fiquet, G., Dewaele, A., Andrault, D., Kunz, M., Le Bihan, T., 2000. Thermoelastic properties and crystal structure of $MgSiO_3$ perovskite at lower mantle pressure and temperature conditions. Geophysical Research Letters 27, 21–24. doi:10.1029/1999GL008397.

Irifune, T., Shinmei, T., McCammon, C.A., Miyajima, N., Rubie, D.C., Frost, D.J., 2010. Iron partitioning and density changes of pyrolite in Earth's lower mantle. Science 327, 193–195. doi:10.1126/science.1181443.

Jackson, I., Niesler, H., 1982. The elasticity of periclase to 3 GPa and some geophysical implications, in: High-Pressure Research in Geophysics, pp. 93–113.

Jackson, I., Rigden, S.M., 1996. Analysis of P-V-T data: constraints on the thermoelastic properties of high-pressure minerals. Physics of the Earth and Planetary Interiors 96, 85–112. doi:10.1016/0031-9201(96)03143-3.

Lundin, S., Catalli, K., Santillán, J., Shim, S.H., Prakapenka, V.B., Kunz, M., Meng, Y., 2008. Effect of Fe on the equation of state of mantle silicate perovskite over 1 Mbar. Physics of the Earth and Planetary Interiors 168, 97–102. doi:10.1016/j.pepi.2008.05.002.

McDonough, W.F., Sun, S.S., 1995. The composition of the Earth. Chemical Geology 120, 223–253. doi:10.1016/0009-2541(94)00140-4.

Shim, S.H., Duffy, T.S., Shen, G., 2000a. The equation of state of $CaSiO_3$ perovskite to 108 GPa at 300 K. Physics of the Earth and Planetary Interiors 120, 327–338. doi:10.1016/S0031-9201(00)00154-0.

Shim, S.H., Duffy, T.S., Shen, G., 2000b. The stability and P—V—T equation of state of $CaSiO_3$ perovskite in the Earth's lower mantle. Journal of Geophysical Research 105, 25955–25968. doi:10.1029/2000JB900183.

Speziale, S., Zha, C.S., Duffy, T.S., Hemley, R.J., Mao, H.K., 2001. Quasi-hydrostatic compression of magnesium oxide to 52 GPa: Implications for the pressure-volume-temperature equation of state. Journal of Geophysical Research 106, 515–528. doi:10.1029/2000JB900318.

Sturhahn, W., Jackson, J.M., Lin, J.F., 2005. The spin state of iron in minerals of Earth's lower mantle. Geophysical Research Letters 32, L12307. doi:10.1029/2005GL022802.

Vilella, K., Shim, S.H., Farnetani, C.G., Badro, J., 2015. Spin state transition and partitioning of iron: effects on mantle dynamics. Earth and Planetary Science Letters 417, 57–66. doi:10.1016/j.epsl.2015.02.009.

Wu, Y., Qin, F., Wu, X., Huang, H., McCammon, C.A., Yoshino, T., Zhai, S., Xiao, Y., Prakapenka, V.B., 2017. Spin transition of ferric iron in the calcium-ferrite type aluminous phase. Journal of Geophysical Research : Solid Earth 122, 5935–5944. doi:10.1002/2017JB014095.

Table 1: Isothermal bulk modulus (K_{T0}) and volume (V_0) at ambient conditions for several compounds.

Compounds	K_{T0} (GPa)	V_0 (cm^3mol^{-1})
MgO	160[a]	11.25[a]
FeO (LS)	150[b]	10.82[b]
FeO (HS)	150	12.18[b]
$MgSiO_3$	261[c]	24.43[c]
$0.85MgSiO_3$-$0.15FeSiO_3$	259 [c]	24.58[c]
$0.915MgSiO_3$-$0.085Fe_2O_3$	237[d]	24.95[d]
$0.90MgSiO_3$-$0.10FeAlO_3$	262[e]	24.80[e]
$0.90MgSiO_3$-$0.10Al_2O_3$	244[e]	24.66[e]
$CaSiO_3$	236[f]	27.45[f]

[a] Speziale et al. (2001).
[b] Fei et al. (2007).
[c] Lundin et al. (2008).
[d] Catalli et al. (2010).
[e] Catalli et al. (2011).
[f] Shim et al. (2000b).

Table 2: Equation of state parameters for lower mantle minerals: Bridgmanite (Bm), Ferropericlase (Fp) and Ca-Perovskite (CaPv).

Parameter	Bm	Fp	CaPv
K'_{T0}	3.7[a]	4[b]	3.9[c]
θ_0, (K)	1100[a]	673[b]	1000[c]
γ_0	1.4[a]	1.41[b]	1.92[c]
q	1.4[a]	1.3[b]	0.6[c]

[a] Fiquet et al. (2000).
[b] Jackson and Niesler (1982).
[c] Shim et al. (2000a).

Table 3: Bulk composition.

	This study		McDonough and Sun (1995)	
	mol%	wt%	Pyrolite (wt%)	CI (wt%)
SiO_2	37.8	44.3	45.0	49.9
MgO	51.6	40.7	37.8	35.15
FeO	5.7	8.0	8.05	8.0
CaO	3.1	3.4	3.55	2.90
Al_2O_3	1.8	3.6	4.45	3.65

Table 4: Chemical composition in mol% of bridgmanite (Bm) and ferropericlase (Fp) in our reference composition.

Bm		Fp	
$MgSiO_3$	0.896	MgO	0.814
$FeSiO_3$	0.037	FeO	0.186
$FeAlO_3$	0.037		
Al_2O_3	0.030		

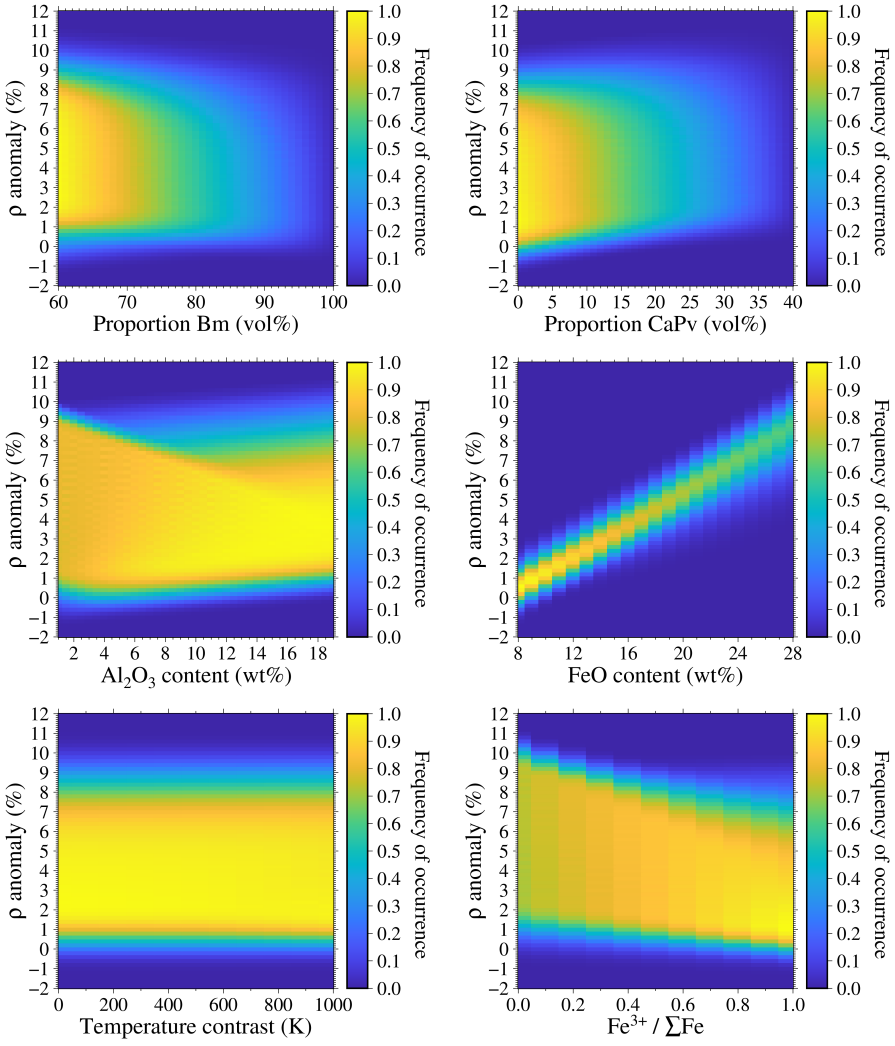

Figure 1: 2D histograms showing the distribution of all the models as a function of the density anomaly (y-axis) for each parameter (x-axis).

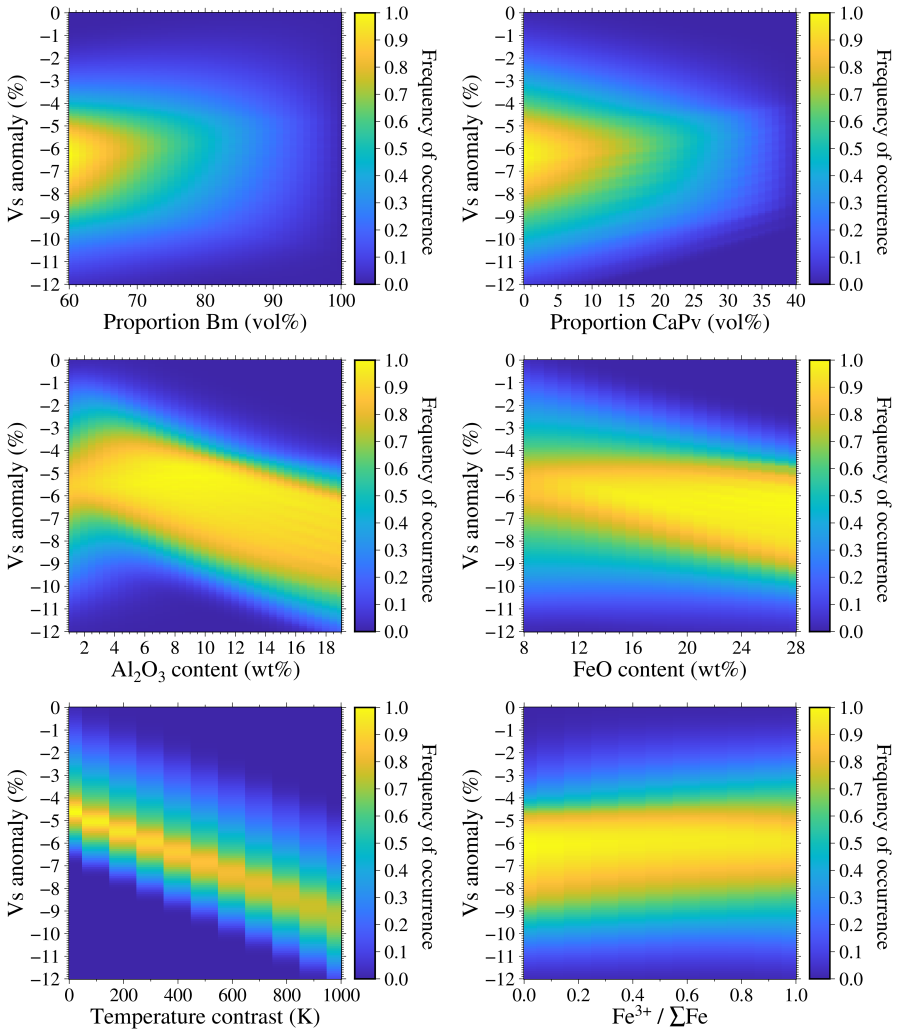

Figure 2: 2D histograms showing the distribution of all the models as a function of the V_S anomaly (y-axis) for each parameter (x-axis).

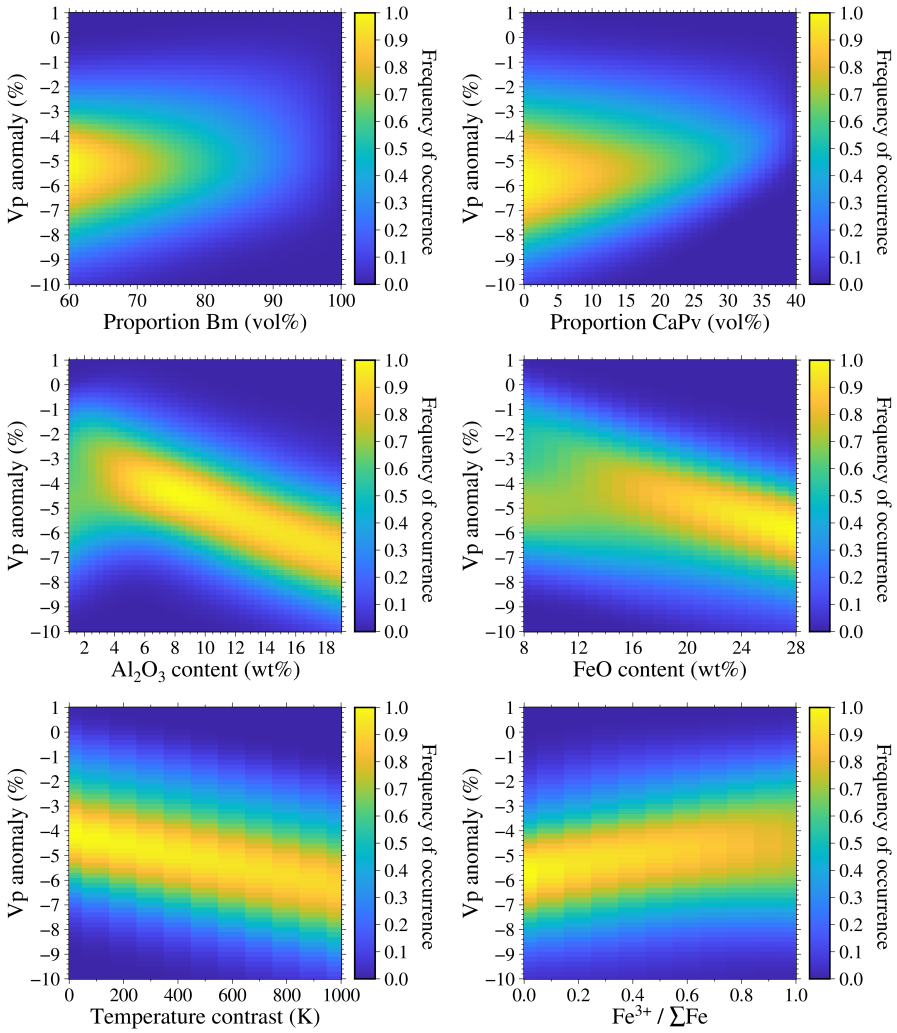

Figure 3: 2D histograms showing the distribution of all the models as a function of the V_P anomaly (y-axis) for each parameter (x-axis).

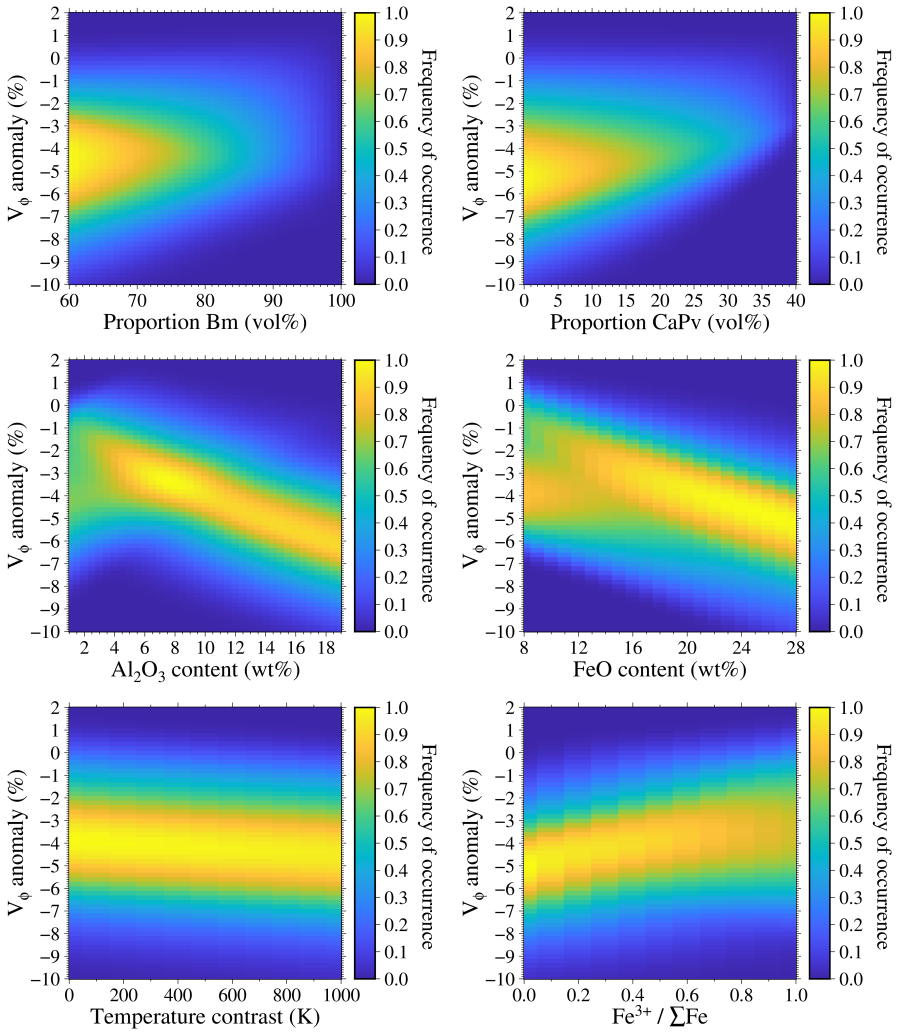

Figure 4: 2D histograms showing the distribution of all the models as a function of the V_ϕ anomaly (y-axis) for each parameter (x-axis).

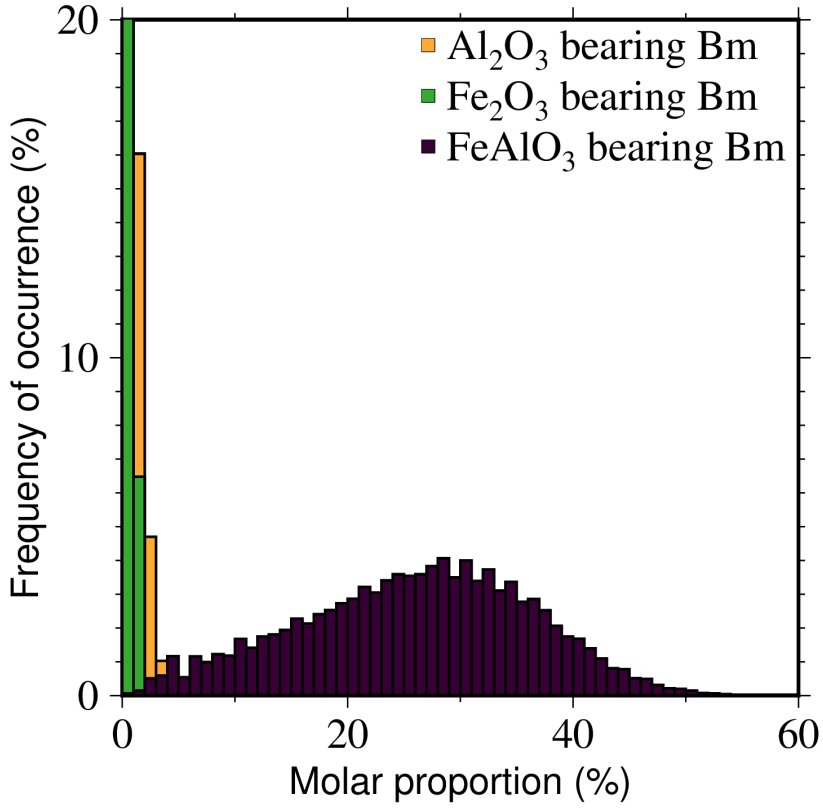

Figure 5: Histograms of the molar proportion of various Bm components for the successful models. For graphical reasons, the y-axis is truncated at 20% whereas the amplitude of the Fe_2O_3 component distribution reaches almost 95%. The results show a clear preference of the $FeAlO_3$ component over the Fe_2O_3 and Al_2O_3 components, which typically remain lower than 5 mol%.

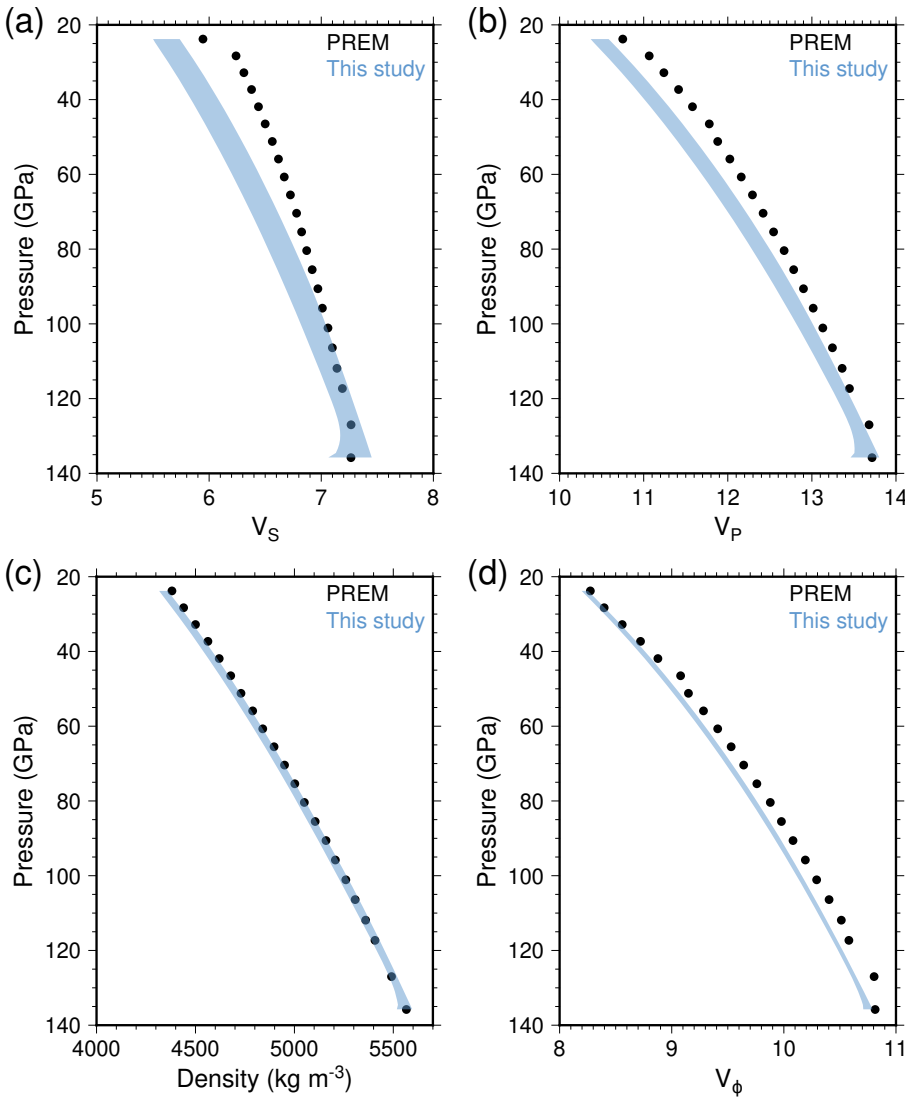

Figure 6: Plots of (a) the S-wave velocity V_S, (b) the P-wave velocity V_P, (c) the density ρ, and (d) the bulk sound velocity V_ϕ as a function of pressure given by PREM (black symbols) and calculated for our reference composition (blue shaded area). The blue shaded area accounts for uncertainties on mantle temperatures (see text for more details).